Thermochimica Acta 742 (2024) 179899

Contents lists available at ScienceDirect

Thermochimica Acta

journal homepage: www.elsevier.com/locate/tca

Pyrolysis of industrial hemp biomass from contaminated soil phytoremediation: Kinetics, modelling transport phenomena and biochar-based metal reduction

Jure Voglar [a,*], Anže Prašnikar [a], Konstantin Moser [b,c], Elisa Carlon [b], Manuel Schwabl [b], Blaž Likozar [a,d,e,f,*]

[a] Department of Catalysis and Chemical Reaction Engineering, National Institute of Chemistry, Hajdrihova 19, 1001 Ljubljana, Slovenia
[b] BEST Bioenergy and Sustainable Technologies GmbH, Inffeldgasse 21b, A-8010 Graz, Austria
[c] University of Natural Resources and Life Sciences, Institute of Chemical and Energy Engineering (IVET), Muthgasse 107/I, 1190 Vienna, Austria
[d] Faculty of Chemistry and Chemical Technology, University of Ljubljana, Večna pot 113, 1001 Ljubljana, Slovenia
[e] Faculty of Chemistry and Chemical Engineering, University of Maribor, Smetanova ulica 17, 2000 Maribor, Slovenia
[f] Faculty of Polymer Technology, Ozare 19, 2380 Slovenj Gradec, Slovenia

ARTICLE INFO

Keywords:
Biomass
Cannabis sativa
Chemical kinetics
Phytoremediation
Pyrolysis

ABSTRACT

Phytoremediation is the use of vegetation for the *in situ* treatment of contaminated environments. After plants have been used for phytoremediation of soils, their biomass can be used for example as value-added products or converted by thermochemical processes. Large-scale application of pyrolysis technology for phytoremediation biomass requires accurate predictive kinetic models and a characterization of the toxicity of the materials produced. The pyrolysis of industrial hemp (*Cannabis sativa* L.) was investigated on a laboratory scale by varying the process conditions and accurately modelled by considering four pseudo-components with first reaction order. The average value of the coefficients of determination is 0.9980. Biomass and biochar were characterized and the main components of the gas phase were monitored. We found Cd, Pb, and Zn in the roots, although in lower amounts than in the soil. Especially the leaves and stems showed negligible traces of these elements, so that these parts can be used directly, even if the hemp was grown on the polluted soil. After pyrolysis, the concentration of pollutants in the solid fraction decreased, which could be attributed to the reduction of metal oxides (or salts) to elemental form and subsequent evaporation. This pyrolysis process has the potential to treat heavy metal-rich biomass, with gas phase purification via condensation, yielding agricultural-grade biochar, CO-rich gas and a highly concentrated heavy metal stream in absorbent material.

1. Introduction

Phytoremediation is the use of vegetation for the *in situ* treatment of contaminated soils, sediments and waters [1]. This technology has proven itself as a more cost-effective, non-invasive, and publicly acceptable way of removing environmental contaminants compared to conventional remediation methods [2]. Organic, nutrient or metal pollutants can be taken up by the roots of plants and sequestered, degraded, immobilized or metabolized on site. Metal-polluted soils, sediments or waters can be remediated by four different mechanisms: (i) phytostabilization, (ii) phytofiltration, (iii) phytovolatilization and (iv) phytoextraction [3].

Some examples of typical plants for heavy metal phytoremediation are *Brassica juncea* L., *Psychotria douarrei* L., *Amanita muscaria* L. and *Brassica napus* L. [4]. Invasive plant species (e.g. the perennial salt marsh grass *Spartina alterniflora* L.) have also been used for phytoremediation [5]. New hyperaccumulating plants can be produced using genetic engineering methods [6]. The industrial hemp plant (*Cannabis sativa* L.) is capable of phytoextraction of heavy metals (e.g. Cd, Cr, Cu, Ni, Pb and Zn) and radionuclides and to reduce the content of polycyclic aromatic hydrocarbons (PAHs) and caesium (Cs) in contaminated soils [7], which is why it can serve as a phytoremediation agent. In addition, the high biomass yield, the long roots and the short life cycle of 180 days make cultivation economically attractive [8]. Further arguments in favor of growing industrial hemp are: (i) pollutants accumulate mainly in its roots, while its stems and seeds (which are used for the production of

* Corresponding authors.
E-mail addresses: jure.voglar@ki.si (J. Voglar), blaz.likozar@ki.si (B. Likozar).

https://doi.org/10.1016/j.tca.2024.179899
Received 20 August 2024; Received in revised form 6 November 2024; Accepted 6 November 2024
Available online 9 November 2024

high-value products) are almost pollutant-free, (ii) the plant has no need for high nitrogen fertilization, (iii) it thrives in a wide range of soils of different soil taxonomy types and (iv) appears to be particularly resistant to soils with high levels of organic and inorganic pollutants [9]. Ideally, phytoremediation with industrial hemp would result in one or more biomass-derived products that yield a net profit. If no profit can be achieved in this manner, other strategies such as composting, compaction, incineration, ashing and pyrolysis should be considered [10]. Some of these strategies (e.g. incineration) are capable of producing large amounts of sustainable bioenergy [11]. Pyrolysis of contaminated hemp biomass, on the other hand, would produce biochar, biooil and syngas, which could be used as valuable resources and fuel [12–14].

The use of biomass from the phytoremediation process is not trivial, as it contains a high concentration of pollutants. Pyrolysis of this biomass either enriches or reduces the content of these pollutants, as it might be susceptible to evaporation at elevated temperature, leading to further complications in the downstream processes. If pollutants remain in the solid phase, they could be extracted by an acidic aqueous solution of HNO_3[15], allowing further use of biochar in agriculture. Another option is to do acid pretreatment-assisted pyrolysis to remove heavy metals before the thermal treatment [16,17]. A careful analysis of the different methods for heavy metal removal is required to find a reliable and cost-effective solution.

The pyrolysis kinetics of phytoremediation biomass was investigated by [18–20]. Du et al. [18] analyzed the non-isothermal kinetics using the Coats-Redfern method under the assumption that the reaction order is equal to 1. They determined different values of the kinetic parameters (pre-exponential factor and activation energy) for different heating rates, which is not an accurate thermodynamic description of pyrolysis. A similar approach was conducted by Asghar et al. [19], who also assumed the 1st reaction order and determined separate kinetic parameters for different values of biomass conversion using three different isoconversional methods: Flynn-Wall-Ozawa method (FWO), Kissenger-Akahira-Sunose method (KAS) and Starink method (STK). In contrast Nath et al. [20], did not assume the 1st reaction order as they used the Sestak-Berggren combined kinetic model and determined separate kinetic parameters for different values of biomass conversion using both the Kissinger method and isoconversional methods (Friedman (FRD), Kissinger-Akahira-Sunose (KAS) and Flynn-Waal-Ozawa (FWO)). The elemental content of pyrolysis obtained biochar from phytoremediation biomass was evaluated by [21–23]. Chami et al. [24] compared flash pyrolysis and slow pyrolysis of heavy metal-contaminated *Sorghum bicolor* L. shoots from phytoremediation. Han et al. [25] proposed an adsorption-pyrolysis technology of phytoremediation biomass to recover Cd and Cu. Many other authors have investigated the pyrolysis of biomass [26–31]. The kinetics of biomass pyrolysis can be described with (i) various isoconversional methods and/or with (ii) least squares fitting in a parallel reaction scheme considering several pseudo-components (usually with three pseudo-components: cellulose, hemicellulose and lignin) [32].

Our research combines both kinetic modelling based on thermogravimetric (TG) measurements and elemental characterization (inductively coupled plasma-mass spectroscopy, ICP-MS) of the produced biochar, which enables us to select suitable pyrolysis process parameters as well as to estimate the quality and toxicity of the biochar. The kinetic modelling with four pseudo-components of first reaction order was, to our knowledge, the first one related to phytoremediation biomass to consider unchangeable kinetic parameters (independent of process conditions and degree of biomass conversion) as well as heat and mass transfer phenomena (internal heat transfer and external mass transport). Therefore, the presentenced integrated kinetics-transport model of phytoremediation biomass pyrolysis is a novelty in the field. In addition, we use attenuated total reflectance-Fourier-transform infrared spectroscopy (ATR-FTIR), scanning electron microscopy coupled with energy dispersive spectroscopy (SEM-EDS), thermogravimetry-Fourier-transform infrared spectroscopy (TG-FTIR), X-ray powder diffraction (XRD) to characterize the biochar and the gas formed.

2. Materials and methods

2.1. Materials

The seeds of Fedora 17 *Cannabis sativa* L. (hemp) were planted on May 16, 2022 on the plot of Slavko Rotar in the Lower Savinja valley, Slovenia at 40 kg/ ha, which was selected due to the elevated heavy metal concentration in the soil. Three soil samples were taken on April 21, 2022 at a depth of 25 cm. The samples were manually crushed using a ceramic pestle and mortar and sieved through a 2 mm mesh sieve. ICP-MS (inductively coupled plasma-mass spectroscopy) measurements were performed after extraction with aqua regia (ISO 11466, 1996) to determine average values of 1.0, 25 and 71 mg/kg DM (dry matter) of cadmium (Cd), lead (Pb) and zinc (Zn), respectively. At the same time, the chemical analysis of the soil was carried out, which revealed that the pH value is 5.4 (ISO 10390:2021), the soil contains 18.8 mg/100 g P_2O_5, 17.3 mg/100 g K_2O and 3.3% organic matter (ISO 17183:2016). Phosphorus and potassium were determined using near infrared reflectance spectroscopy (NIRS) after ammonium lactate extraction [33].

The entire cultivated hemp biomass was harvested on September 13, 2022. The hemp plants therefore grew for 120 days, which is consistent with both the growth cycle from May to September [34] and the duration of the vegetation cycle of 120 to 130 days [35]. The cultivated plants were dug up and cut/divided according to different parts: roots, stems, leaves and flowers. (The flowers were not tested in this work as they represent a relatively small proportion of the total biomass of the industrial hemp plant.) The roots were washed with water to remove the remaining soil and air-dried. Finally, the biomass was dried at 35°C for three days to remove the moisture content of the biomass. The dried hemp is referred to in the paper as hemp-fresh, as opposed to hemp-char, which refers to the samples after pyrolysis. Wherever a particular part of the plant has been used, we have labeled the sample, e.g. stem-fresh or stem-char.

2.2. Thermogravimetry

The biomass samples were prepared by grinding the dried biomass particles with a kitchen blender to < 0.5 mm (or manual cutting in the case of the 2 mm and 1 mm fractions) and weighing 4-13 mg of dry hemp biomass into the weighed 150 µl alumina crucibles without lids. The pyrolysis process of the hemp biomass was monitored by thermogravimetry (TG) on the PerkinElmer EGA 4000 (Waltham, Massachusetts, USA) instrument in nitrogen (N_2) atmosphere at volumetric flow rates (Q) of 5, 10, 25 and 50 ml/min. Measurements were also performed at heating rates (β) of 5, 10, 15, 20 and 25 K/min, where the N_2 flow rate was 50 ml/min. Hemp stems with particle sizes (δ) of 2, 1 and < 0.5 mm were tested. The pyrolysis of plant parts: roots, stems and leaves were also evaluated. The measurements were always carried out from 40 to 700°C with a holding time of 60 minutes at the final temperature of 700°C. Holding the biochar at 700°C resulted in a mass loss between 0.7 and 1.7% of the initial mass. The TG experimental matrix is presented in Table 1.

2.3. Kinetic modelling of pyrolysis

The pyrolysis kinetic model fitting was carried out in the Python programming language using the Spyder integrated development environment (IDE). The pyrolysis model, which accounts for internal heat transfer and chemical kinetics, was formulated for four pseudo-components (i): volatiles ($i = 1$), hemicellulose ($i = 2$), cellulose ($i = 3$) and lignin ($i = 4$). The volatiles represented the low temperature volatiles and the remaining hydroponically present water originating from the ambient humidity, while the remaining three pseudo-components (hemicellulose, cellulose and lignin) were modelled (as

Table 1
TG experimental matrix.

#	β (K/min)	Q (ml/min)	*Plant part* (/)	δ (mm)
1	5	5	stems	< 0.5
2	5	10	stems	< 0.5
3	5	25	stems	< 0.5
4	5	50	stems	< 0.5
5	10	50	stems	< 0.5
6	15	50	stems	< 0.5
7	20	50	stems	< 0.5
8	25	50	stems	< 0.5
9	5	50	stems	2
10	5	50	stems	1
11	5	50	roots	< 0.5
12	5	50	leaves	< 0.5

pseudo-components) as in most literature on biomass pyrolysis, e.g. [32]. The measured TG quantities of time, mass and temperature were modelled using the following set of Eqs..

The pseudo-component's conversion during pyrolysis is defined by Eq. 1, where $m_{i,s}$ is the initial mass, $m_{i,f}$ is the final mass and m_i is the current mass.

$$X_i = \frac{m_{i,s} - m_i}{m_{i,s} - m_{i,f}} \tag{1}$$

The total biomass conversion is the sum of the pseudo-component's conversions X_i multiplied by their mass fractions w_i (Eq. 2).

$$X = \sum_{i=1}^{4} w_i X_i \tag{2}$$

The measured temperature T_m at the interface between the furnace and the alumina crucible was modelled using the first order differential Eq. (Eq. 3), where β is the heating rate.

$$\frac{dT_m}{dt} = \beta \tag{3}$$

The internal heat transfer was modelled with the first order differential Eq. (Eq. 4), where T is the temperature of the sample, α is the sample's thermal diffusivity and h is the height of the sample in the crucible.

$$\frac{dT}{dt} = \frac{2\alpha}{h^2}(T_m - T) \tag{4}$$

The kinetics were modeled using the first order differential Eq. (Eq. 5) in the cases where external mass transport limitations were neglected (at the maximum N_2 flow rate of 50 ml/min; TG data # 4 to 12), where k_i is the reaction rate constant, A_i is the pre-exponential factor, $E_{a,i}$ is the activation energy, and R is the ideal gas law constant of 8.314 J/(mol·K).

$$\frac{dX_i}{dt} = k_i(1 - X_i) = A_i e^{\left(-\frac{E_{a,i}}{RT}\right)}(1 - X_i) \tag{5}$$

On the other hand, in the cases where the external mass transport limitations could not be neglected (at the lower N_2 flow rates; TG data # 1 to 3), the kinetics were modelled using the two first order differential Eqs. (Eqs. 6 and 7), where $X_{a,i}$ is the kinetics limited pseudo-component's conversion, X_i is the kinetics and transport limited pseudo-component's conversion, k_l is the external mass transport coefficient, and a is the ratio of surface area to volume of the pyrolyzed material.

$$\frac{dX_i}{dt} = k_l a(X_{a,i} - X_i) \tag{6}$$

$$\frac{dX_{a,i}}{dt} = k_i(1 - X_{a,i}) = A_i e^{\left(-\frac{E_{a,i}}{RT}\right)}(1 - X_{a,i}) \tag{7}$$

For the entire kinetic modelling, the 1st reaction order was assumed for the pyrolysis of the four pseudo-components, which is consistent with the other literature studies, e.g. [18,19].

The differential Eqs. were solved using the scipy.integrate.odeint function, while the numerical data fitting was performed using the scipy.optimize.curve_fit function. The modeling steps are shown in Fig. 1.

The initial ratio of the hemicellulose:cellulose:lignin pseudo-components (20:59:21) was determined from the literature [36,37]. The pre-exponential factors were set to $1{\cdot}10^{12}$ 1/s, as the estimated values for the high vibrational frequencies of the bonds were in the range between $1{\cdot}10^{12}$ and $1{\cdot}10^{13}$ 1/s. The initial estimate of the thermal diffusivity of the hemp biomass was equal to $5{\cdot}10^{-7}$ m^2/s [38].

2.4. Material characterizations

2.4.1. Density measurements

The density of the biomass was estimated by measuring the volume and mass of the samples. Approximately 0.25 grams of biomass was placed in a glass vial, the volume was determined and the biomass was weighed on the laboratory scale with a stated accuracy (e) of 0.001 g. The estimated densities were 92, 71 and 83 kg/m^3 for roots, stems and leaves, respectively. These densities were used to estimate the height (h) of the biomass samples.

2.4.2. X-ray powder diffraction (XRD)

Samples were analyzed by powder X-ray diffraction (XRD) using the PANalytical X'Pert Pro (Almelo, Netherlands) instrument. The CuKα1 radiation source was used for scanning from 10 to 80°. The diffractogram analyzes were performed using HighScope Plus with PDF-5 database.

2.4.3. Scanning electron microscopy coupled with energy dispersive spectroscopy (SEM-EDS)

Scanning electron microscopy was performed using the HR-SEM Zeiss Supra 35 VP (Oberkochen, Germany) instrument coupled with an EDS detector. EDS analyzes were performed at 20 kV, aperture size 120 μm for 1 min at three positions for a single sample. SEM imaging was performed on samples mounted on a carbon tape and imaged at 1 kV (high magnification) with a 30 μm secondary electron detector. To avoid a significant background contribution, large individual particles were analyzed by EDS. Prior to analysis, the fresh samples were coated with a 10 nm thick gold layer, while the char samples were already conductive enough for SEM observation.

2.4.4. Attenuated total reflectance-fourier-transform infrared spectroscopy (ATR-FTIR)

The ATR-FTIR analyzes were performed with the Spectrum Two 135 from PerkinElmer (Waltham, Massachusetts, USA). Scanning was carried out with a MIR detector in a wavenumber range from 400 cm^{-1} to 4000 cm^{-1} with a step of 4 cm^{-1} (accumulation of 32 scans for each step).

2.4.5. Thermogravimetry-fourier-transform infrared spectroscopy (TG-FTIR)

Measurements of gas composition during pyrolysis were performed with TG-FTIR (FTIR-Spectrum 3, PerkinElmer (Waltham, Massachusetts, USA), TG EGA 4000, PerkinElmer (Waltham, Massachusetts, USA)). Approximately 15 mg of fresh stems was placed in the cup in the cell, then purged with N_2 and heated from 40 to 700°C at a rate of 5 K/min. The gas composition was monitored with a MIR detector in the same wavenumber range and with the same step size as ATR-FTIR, using only 4 scans for averaging in a single time step.

2.4.6. Inductively coupled plasma-mass spectroscopy (ICP-MS)

The ICP-MS analyzes were performed at the National Laboratory of Health, Environment and Food (NLZOH). Approximately 0.3 g of the dried sample was digested according to the standard (SIST EN

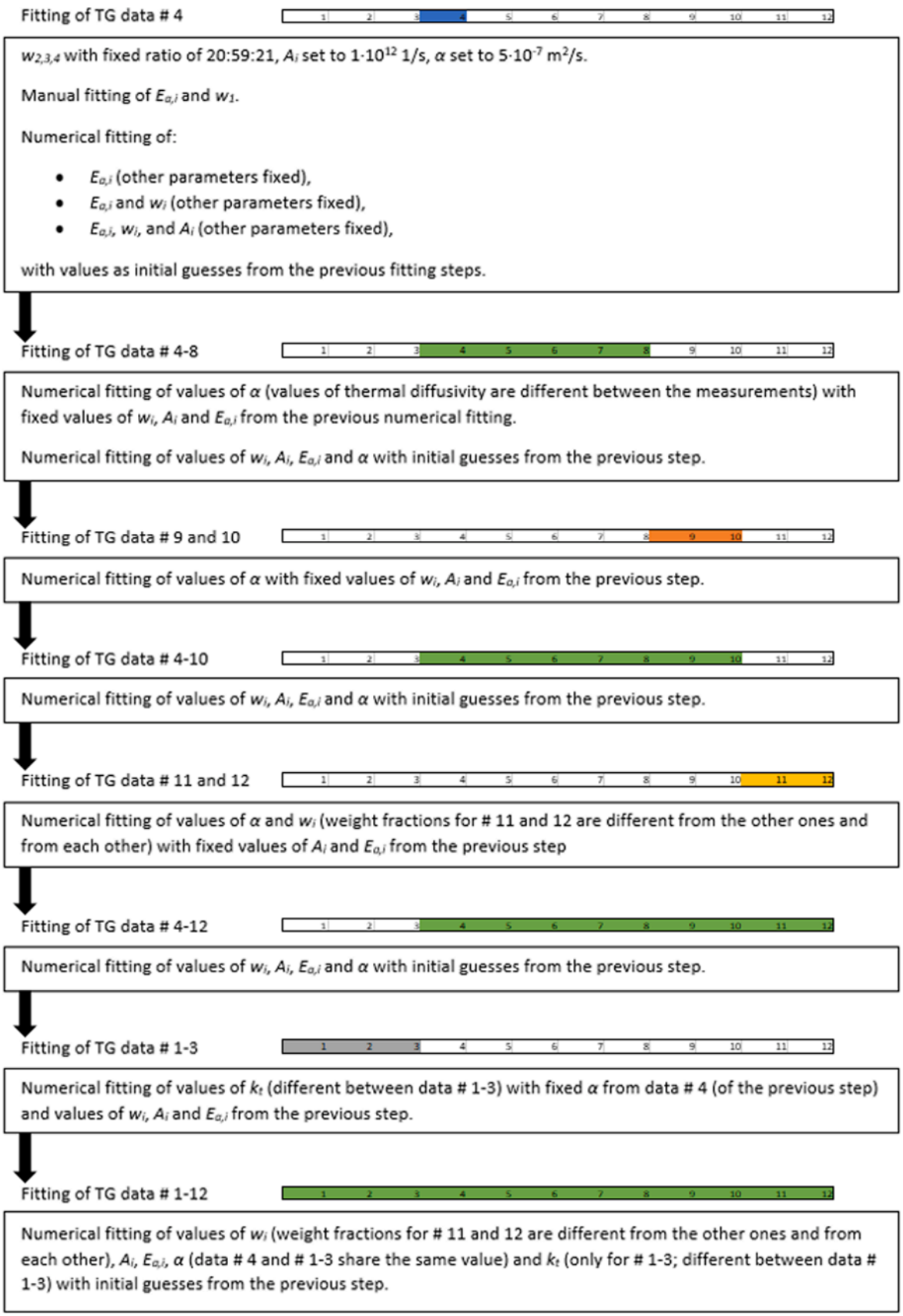

Fig. 1. Scheme for determining the pyrolysis kinetic parameters (A_i, $E_{a,i}$), the biomass pseudo-component compositions (w_i) and the mass transport coefficients (k_t).

13656:2020) and then the concentration was determined by ICP-MS according to the standard (SIST EN 16171:2017). To obtain a larger amount of biochar for ICP-MS, we performed pyrolysis in the tube furnace at a heating rate of 5 K/min to 700°C in N_2.

3. Results and discussion

3.1. Influence of the carrier gas flow rate on pyrolysis

The influence of the carrier gas flow rate was observed at four different flow rates of nitrogen: 5, 10, 25 and 50 ml/min. The heating rate was maintained at 5 K/min, while the input biomass material used in all cases was the ground hemp stems. The results presented in the Fig. 2 (a, b) indicate the general trend of an increase in mass loss with increasing nitrogen flow rate. This can be attributed to enhanced external mass transport of the evolved gases form the heated material at higher flow rates. At a flow rate of 25 ml/min (# 3), there is only a slight deviation from this trend, which is due to the height difference of the sample (*h*).

External mass transfer plays an important role in the pyrolysis of the ground hemp stems and was modelled using Eqs. 6 and 7 (in cases # 1 to 3). The mass transport of volatiles produced during pyrolysis is rarely modelled in the literature. We have found only a few articles [39,40] with models for the mass transport of gasses produced during pyrolysis.

3.2. Influence of the heating rate on pyrolysis

The heating rates studied were: 5, 10, 15, 20 and 25 K/min, while the nitrogen flow rate was kept at 50 ml/min and the pyrolyzed biomass material was ground hemp stems. The general trends observed here are: (i) the measured weight curves shift to higher temperatures as the heating rate is increased (Fig. 2 c), (ii) the values of the remaining weights are higher at higher heating rates (Fig. 2 c), and (iii) the peaks of the mass loss rate tend to shift to slightly higher temperatures at the higher heating rates (Fig. 2 d).

These results indicate the significance of internal heat transfer (resistance) in the pyrolysis of the ground hemp stems, which was modelled using Eqs. 3 and 4. Most previous studies do not consider internal heat transfer and therefore model different cases of heating rates with separate sets of kinetic parameters (pre-exponential factors and activation energies), e.g. [18]. The resulting activation energies are sometimes referred to as apparent activation energies [41], which is a more accurate description as they do not model the actual chemical kinetics of the pyrolysis reactions, but fit the data without accounting for the multitude of other physical phenomena occurring related to heat and mass transfer. Another approach by introducing a parameter called temperature correction, which is a temperature offset depending on the applied heating rate, was used by Cardona et al. [40] for modelling bitumen pyrolysis at different heating rates.

3.3. Influence of biomass particle size on pyrolysis

The variation of the particle size of 2 mm, 1 mm and ground state (< 0.5 mm) of the hemp stems was investigated at a heating rate of 5 K/min and a nitrogen flow rate of 50 ml/min. The results indicate a faster general mass loss with smaller particles (Fig. 3 a). This can be explained by variations in material properties, e.g. density and thermal diffusivity, which influence both internal heat transfer and internal mass transfer (resistance).

The internal mass transfer was not modelled separately, while the model accounted for the differences in material properties with the variation in biomass particle size (which affects the internal heat transfer). This approach was still a more accurate description of the actual phenomena than if both the heat and mass transfer phenomena during pyrolysis were completely excluded, which is the common practice in the available literature e.g. [41]. On the other hand, some of the authors have modelled the internal mass transfer during pyrolysis using Darcy's law, e.g. [39,42].

3.4. Influence of the hemp plant part on pyrolysis

The TG investigation of the different hemp plant parts: roots, stems

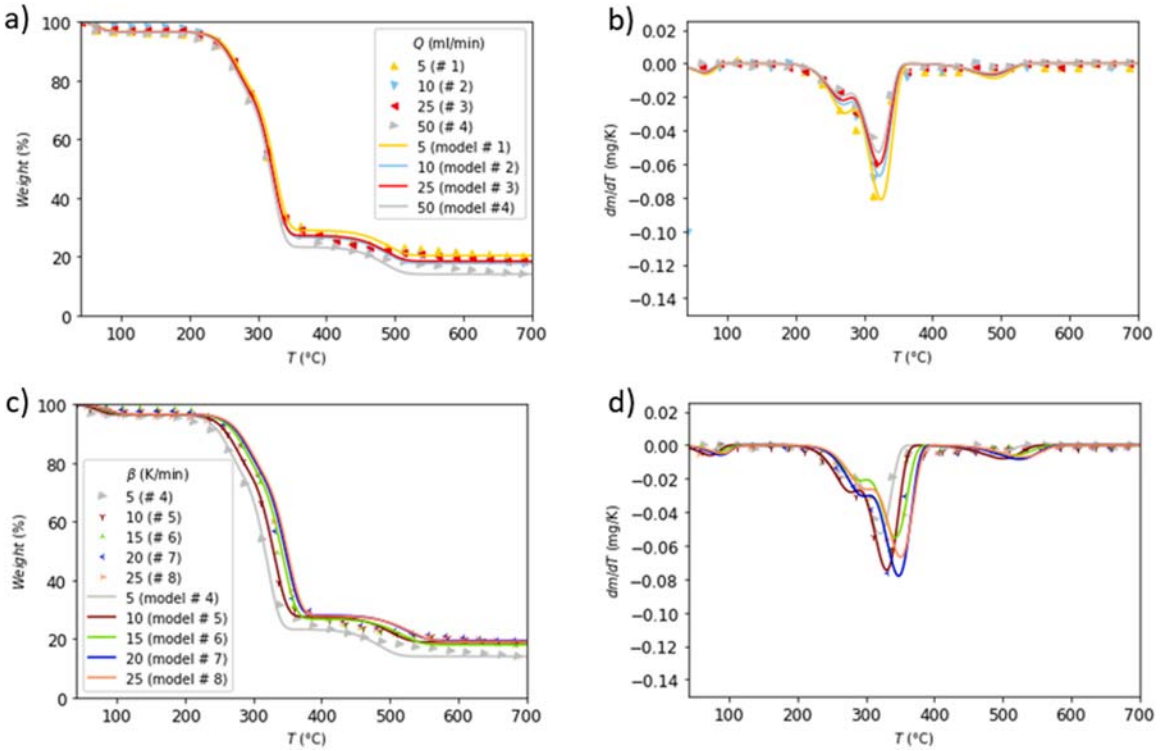

Fig. 2. Relative weight and mas loss rate in the temperature domain at different carrier gas flow rates (a, b) and heating rates (c, d).

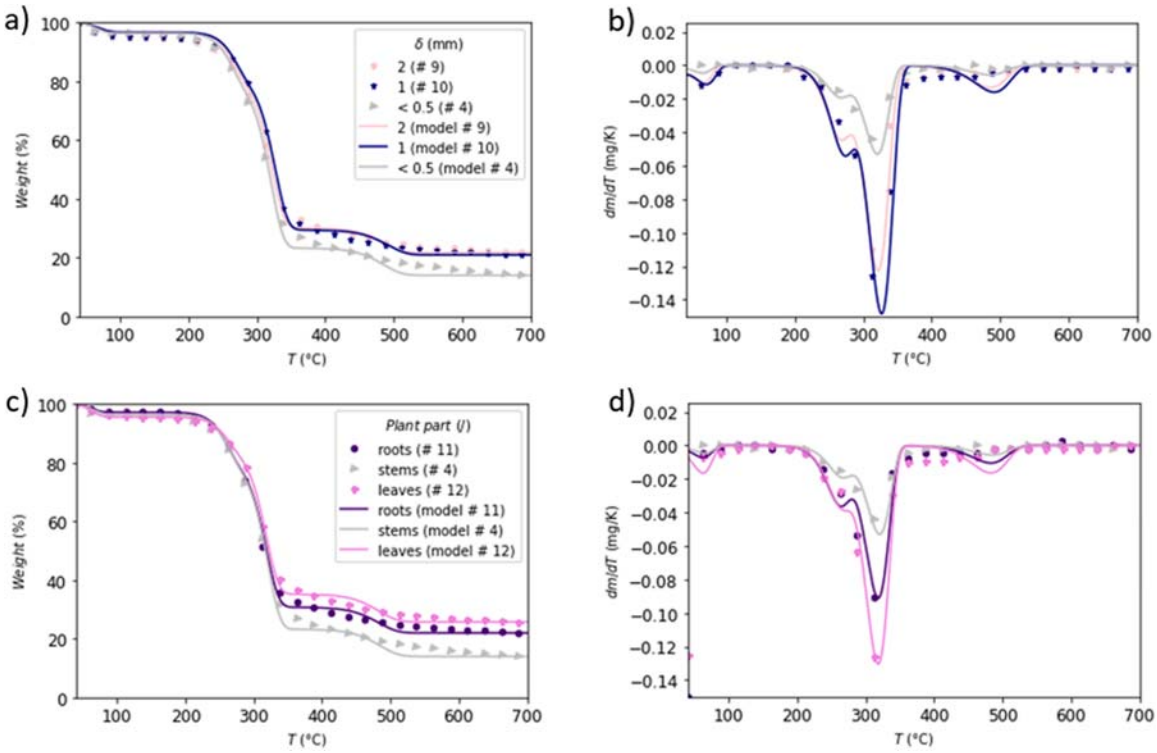

Fig. 3. Relative weight and mass loss rate in the temperature domain for different particle size fractions (a, b) and hemp plant parts (c, d).

and leaves took place at a heating rate of 5 K/min and a nitrogen flow rate of 50 ml/min. The highest overall mass loss was observed in the stems, slightly less in the roots and the slowest overall mass loss was observed in the leaves (Fig. 3 c). On the other hand, the peak mass loss rates (Fig. 3 d, all at ∿ 320°C) were highest in leaves, slightly lower in roots and lowest in stems.

This TG dataset was modelled by varying the mass fractions of the pseudo-components and the material properties, e.g. thermal diffusivities.

3.5. Pyrolysis kinetic parameters and pseudo-component compositions of the biomass

The kinetic parameters of hemp pyrolysis are summarized in Table 2. The values of the activation energy of the decomposition of the pseudo-components are similar to the values reported in the literature for hemicellulose (132.9 kJ/mol, [43]), cellulose (vegetal cellulose: from 153.3 to 169.5 kJ/mol, [44]) and lignin (174.7 kJ/mol for a 1st order model with Gaussian distribution of the Distributed Activation Energy Model (DAEM), [45]).

The pseudo-component compositions of the biomass are presented in Table 3. The pseudo-component composition of the hemp stems (# 1 to 10) is within the range 20 to 40% bast fibers and 60 to 80% hurds; the compositions of hemp bast fibers and hurds are presented in [36]. The roots exhibited a slightly higher concentration of hemicellulose, a slightly lower cellulose content and a slightly higher lignin concentration (compared to the stems), indicating a slightly higher proportion of hurds, the woody part of the hemp plant. The leaves had a significantly lower concentration of hemicellulose, a slightly higher cellulose content and a higher concentration of lignin (compared to the stems), which is more similar to bast fibers than hurds and indicates a higher bast fiber content.

Table 2
Kinetic parameters of hemp pyrolysis for four pseudo-components (i): volatiles ($i = 1$), hemicellulose ($i = 2$), cellulose ($i = 3$) and lignin ($i = 4$).

$E_{a,1}$ (kJ/mol)	62.8
$E_{a,2}$ (kJ/mol)	136.8
$E_{a,3}$ (kJ/mol)	161.6
$E_{a,4}$ (kJ/mol)	176.3
A_1 (1/s)	$3.31 \cdot 10^{7}$
A_2 (1/s)	$1.23 \cdot 10^{11}$
A_3 (1/s)	$8.61 \cdot 10^{11}$
A_4 (1/s)	$4.63 \cdot 10^{9}$

Table 3
Biomass pseudo-component (i) compositions: volatiles ($i = 1$), hemicellulose ($i = 2$), cellulose ($i = 3$) and lignin ($i = 4$).

#	1 to 10	11	12
w_1 (/)	0.042	0.036	0.059
w_2 (/)	0.182	0.200	0.135
w_3 (/)	0.669	0.652	0.678
w_4 (/)	0.108	0.112	0.127

The values of the external mass transport coefficients, the thermal diffusivities and the coefficients of determination (R^2) of the fitted kinetic models are listed in Table 4. The values of the external mass transport coefficients ($k_l a$) are in the same order of magnitude and decrease monotonically with decreasing nitrogen flow rate, which was to be expected since the external mass transfer is weakened at lower N_2 flow rates. The average value of the thermal diffusivity is $1.97 \cdot 10^{-6}$ m^2/s, while the minimum and maximum values are $5.68 \cdot 10^{-8}$ and $8.96 \cdot 10^{-6}$ m^2/s, respectively. The values of the thermal diffusivity are therefore in three orders of magnitude, which was not difficult to expect, as the material (thermal) properties usually vary with temperature, particle size (porosity) and material composition (degree of conversion). Moreover, in some cases (# 5 to 10), the thermal diffusivity was the only free parameter to fit the experimental TG data and could take values that do not reflect the actual thermal properties of the material being pyrolyzed, but could incorporate other effects such as non-uniform particle size and internal mass transfer. The average value of the coefficients of

Table 4
External mass transport coefficients, thermal diffusivities and coefficients of determination.

#	1	2	3						
$k_f a$ (1/s)	$2.58{\cdot}10^{-1}$	$4.07{\cdot}10^{-1}$	$5.30{\cdot}10^{-1}$						
α (m^2/s)	$5.68{\cdot}10^{-8}$	$5.68{\cdot}10^{-8}$	$5.68{\cdot}10^{-8}$						
R^2 (/)	0.9969	0.9980	0.9986						
#	4	5	6	7	8	9	10	11	12
α (m^2/s)	$5.68{\cdot}10^{-8}$	$8.96{\cdot}10^{-6}$	$9.60{\cdot}10^{-8}$	$2.95{\cdot}10^{-7}$	$3.55{\cdot}10^{-7}$	$2.64{\cdot}10^{-7}$	$1.41{\cdot}10^{-7}$	$7.51{\cdot}10^{-6}$	$5.80{\cdot}10^{-6}$
R^2 (/)	0.9968	0.9983	0.9978	0.9988	0.9986	0.9972	0.9983	0.9983	0.9982

determination is 0.9980, while the minimum and maximum values are 0.9968 and 0.9988, respectively. Therefore, the presented kinetic modelling of hemp pyrolysis has sufficient agreement with the experimental measurements performed on a laboratory scale. A detailed error analysis can be found in Figure A.1 and Table A.1.

A high degree of accuracy was not the main goal of our modelling. Besides achieving sufficient accuracy, our goal was to develop a kinetic model that is robust and considers all relevant physical (heat and mass transfer) and chemical phenomena (kinetics). If the main aim of kinetic modelling is to achieve a high degree of accuracy, differential and integral isoconversional methods might perform better. Highly accurate kinetic modeling concerning combustion of waste berry pomace was performed using AKTS (Advanced Kinetics and Technology Solutions) software with FWO and ASTM E-698 methods [46]. Friedman (FRD), FWO and ASTM E-698 methods were used for thermokinetic modelling of cellulose decomposition under isothermal, non-isothermal and stepwise heating [47]. Kinetic predictions under isothermal conditions for the pyrolytic conversion of cotton stalks were made using the (AKTS) software [48].

3.6. Characterization results of biomass, biochar and gaseous products

3.6.1. SEM-EDS analysis

The determined atomic O/C ratio of fresh hemp is between 0.26-0.55 and decreases to 0.07-0.16 during pyrolysis (Table 5), which is common for biomass treated at above 700°C [49]. A similar O/C ratio is observed in the biochar of stems and leaves, 0.14 ± 0.01 and 0.16 ± 0.06, respectively, while roots (sample 11) contain about half of the oxygen, which could be related to a less porous structure, as observed in Fig. 4 (c, d). As expected, the concentration of potassium and calcium increases during pyrolysis, with stems containing about 3% and 1% K and P, respectively. Hemp is also interesting because it contains lower amounts of sulfur compounds [50], especially in the stem (Appendix A, Table A.2), as desulfurization of the gaseous products is crucial for a possible catalytic conversion to e.g. MeOH [51]. A higher O/C ratio and a lower content of micronutrients in fresh stems than in leaves and roots may be the reason for the lower biochar yields observed in Fig. 3 (c) after treatment at 700°C.

Table 5
The average elemental composition of the samples determined by the SEM-EDS technique. Elements that were qualitatively confirmed using this technique and whose content is below 1 wt% can be found in Appendix A, Table A.2. The standard deviations are provided.

	Hemp-char			Hemp-fresh		
	Roots (11)	Leaves (12)	Stems (4)	Roots	Leaves	Stems
O/C wt. (/)	0.10 ± 0.02	0.22 ± 0.08	0.18 ± 0.01	0.50 ± 0.05	0.34 ± 0.01	0.73 ± 0.01
O/C at. (/)	0.07 ± 0.02	0.16 ± 0.06	0.14 ± 0.01	0.40 ± 0.04	0.26 ± 0.01	0.55 ± 0.01
C (wt. %)	84 ± 3	76 ± 6	81 ± 2	63 ± 3	70 ± 1	57 ± 1
O (wt. %)	8 ± 2	17 ± 5	15 ± 1	34 ± 3	24.0 ± 0.5	42.0 ± 0.3
K (wt. %)	6 ± 1	6 ± 1	3.1 ± 0.6	1.2 ± 0.1	3.6 ± 1.0	0.5 ± 0.2
Ca (wt. %)	1.0 ± 0.5	1.2 ± 0.8	0.9 ± 0.3	0.6 ± 0.3	1.2 ± 0.4	0.3 ± 0.1
Rest (wt. %)	1	0	0	1.2	1.2	0.2

Fig. 4 shows the morphology of the fresh samples (a, c, e) and the pyrolyzed samples (b, d, f). We see that the structure of the stem (Fig. 4 a, b) remains very similar after pyrolysis with cell sizes between 10-50 μm. The main difference is the reduced thickness of the cell walls and a much smoother texture due to the decomposition of unstable compounds. The structure of the roots before and after pyrolysis (Fig. 4 c, d) is less ordered, contains more elements and is less porous. Visually, the leaves are greener than the stems, as they represent the outer parts of the plant. Using SEM imaging, we can see that the thickness of the dried leaves is between 40-60 μm, with similar dimensions also observed in the biochar samples. The SEM-EDS mapping (Fig. 4 g, h, i) shows the Ca and K distribution, with potassium being more evenly distributed, although it is present in higher concentration (3%). A different morphology of the different plant parts apparently has no influence on the decomposition kinetics, as can be seen in Fig. 3 (c, d).

3.6.2. ICP-MS analysis for the determination of micropollutants

One of the critical factors in the production of biochar is to increase the concentration of elements in the solid phase, as these can be less volatile and potentially toxic. Conversely, volatile and toxic elements can end up in the gas phase and pollute the environment or potentially cause damage to equipment. As the hemp grew on soil with high levels of Zn, Cd and Pb, we tested the individual plant parts and found that the levels in the upper plant parts (stems and leaves), were below the limit of detection, as can be seen in Table 6, which is also consistent with previous results [9]. In contrast, the roots contain significant amounts of Zn, Pb and Cd, which is similar as in the literature [8]. However, the concentration is lower than in the soil, which makes this plant species less effective for phytoremediation of soil polluted with the investigated metals, especially since no Cd, Pb or Zn was found in the upper part of the plant. There are large discrepancies in heavy metal extraction performance with different plants [52]. The biomass of the grapevine contains significantly lower concentrations of Cd, Pb and Zn than the soil. On the other hand, the Zn content in the biomass of *Coronopus didymus* L. is more than three times higher than in the soil on which it grew. In addition to the plant species (and its growth time and season), environmental conditions such as soil properties and weather can also influence heavy metal accumulation. The leaching of Zn and (to a lesser extent) Pb from the soil could occur during the growth of the plant due to rainfall [53,54]. In the case of Cd, significant leaching is not expected as the soil pH is 5.4 and no leaching was observed at pH above 4 [53]. We can observe that the Cd concentration in the roots is about 10 times lower than the concentration in the soil, indicating a poor absorption of this element. However, this does not exclude hemp-based phytoremediation for the cases with other pollutants. The analysis of the biochar produced from the roots gave interesting results with a much lower concentration than theoretically expected if Zn (half of the expected value), Cd and Pb (lower than in fresh material and too low for determination) would remain in the solid phase (at solid mass reduction to 22%). A reduction of Zn, Cd and Pb content in the solid phase was also observed in the pyrolysis of sunflower [55]. Therefore, in general, any

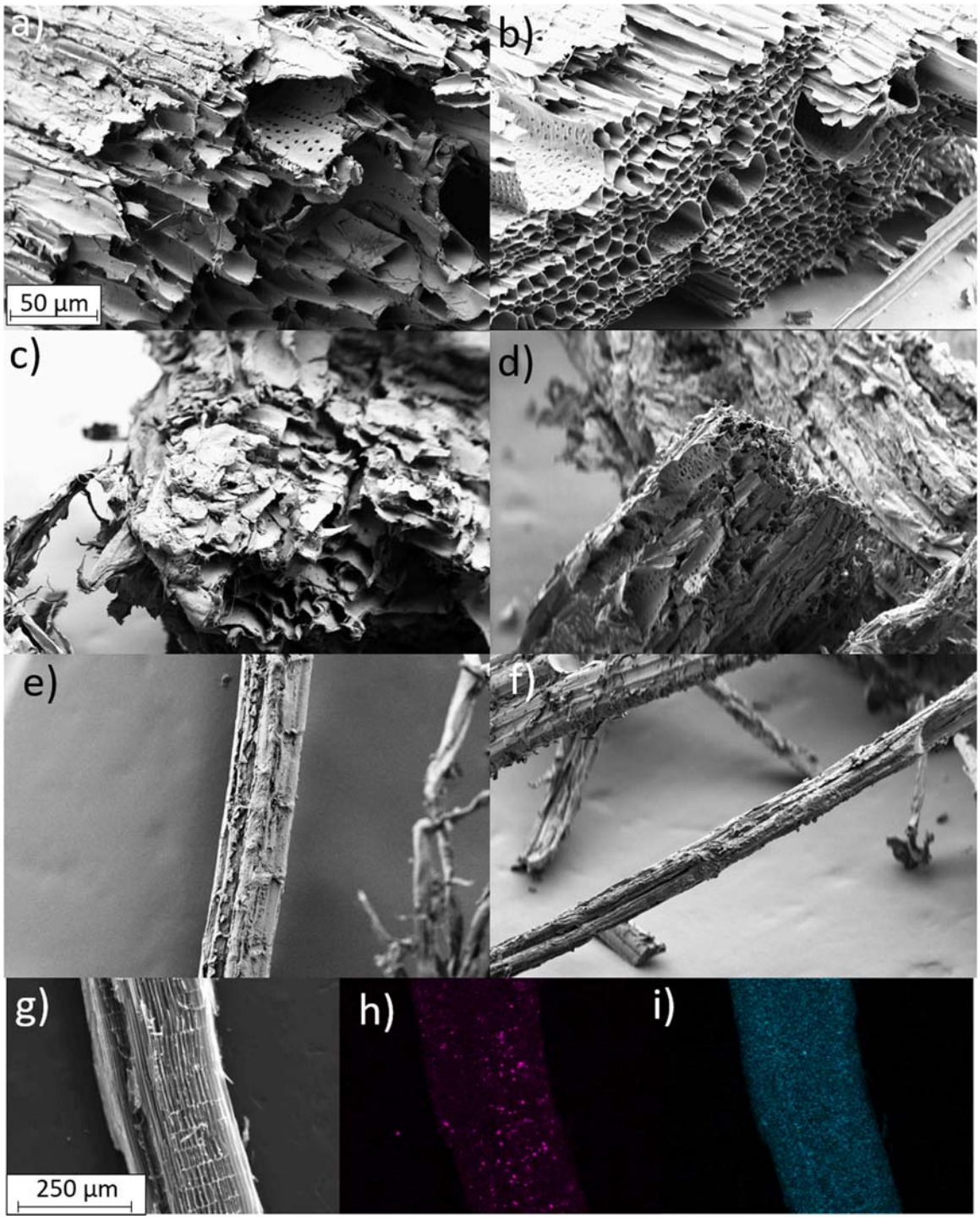

Fig. 4. SEM analyzes of fresh and charred hemp stems (a, b), fresh and charred hemp roots (c, d), fresh and charred hemp leaves (e, f), SEM and SEM-EDS mapping of charred hemp stems (g-i) with Ca (h) and K (i) distributions. The magnification of (a-f) is 1000× and (g-i) is 300×.

type of biochar can be used in agriculture, even if the biomass and soil are contaminated, although gas treatment might be required. The reduced amount of Zn, Cd and Pb could be connected with evaporation. All, Zn, Pb and Cd are probably in the form of oxides or salts with high melting points (ZnO melting point 1975°C, PbO melting point 886°C, CdO sublimation point at 1559°C). During pyrolysis, however, reducing gasses are formed, in particular carbon monoxide (CO, while CH_4 and H_2 are present), which can partially reduce ZnO to Zn at 300°C [56]. Cd and Pb are even more electronegative, with the reduction of PbO at 400°C in H_2 [57]. The melting points of the metals are much lower (Pb 327°C, Cd 321°C, Zn 419°C), and significant evaporation occurs at these temperatures. Therefore, these pollutants could (partially in the case of Zn) exit the pyrolysis section in elemental form. Ideally, the heavy metals could be concentrated on the filter absorbent at lower temperatures so that both the gas and biochar streams remain clean. In our case, we did not pass the gaseous products through the sorbent to capture the investigated metals and analyze the sorbent. However, this would be important to close the mass balance. In general, there is an extremely large difference between the measured values and the theoretical values without evaporation and the change cannot be due to minor errors (e.g. in

Table 6
Determination of micropollutants by inductively coupled plasma-mass spectrometry. The line »Roots-theoretical« represents the values that should be determined if selected elements would not evaporate (22% mass remaining after pyrolysis).

Sample		Concentration (mg/kg dry matter)		
		Zn	Cd	Pb
Soil		71	1	25
Hemp-Fresh	Stems	<13	<0.1	<1
	Leaves	<13	<0.1	<1
	Roots	18 ± 3	0.25 ± 0.05	2.8 ± 0.4
Hemp-Char	Roots	46 ± 6	<0.1	<1
	Roots-theoretical	82 ± 14	1.1 ± 0.2	13 ± 2

weighting). In addition, a decrease in metal content was also observed in the literature [58], where they showed 100% volatilization of Cd during pyrolysis of rubber tire particles (100 μm) at 600°C, while for Zn and Pb they showed an increase in volatilization rate with temperature increase and also complete volatilization at 900°C. However, the use of larger organic particles could decrease the volatilization rate due to mass transfer limitations.

Based on the concentrations of Cd, Pb and Zn in Stem-Fresh, Leaves-Fresh and Roots-char, any part of the plant can be used after pyrolysis at investigated conditions as animal feed or as fertilizer in agriculture. The limits for feed-grade biochar are Pb < 10 mg/kg DM and Cd < 1 mg/kg DM [59]. According to the European biochar certificate (EBC), biochar for animal feed (EBC-FeedPlus) should contain Pb < 10 mg/kg DM, Cd < 0.8 mg/kg DM and Zn < 200 mg/kg DM [60]. Guidelines and national regulations should be followed to avoid possible undesirable environmental contamination when using biochar.

3.6.3. X-ray powder diffraction (XRD)

The diffractograms of fresh and pyrolyzed biomass are shown in Fig. 5 (a). Untreated samples exhibit characteristic peaks at 22.2° related to (200) and a broad peak between 14.9° and 16.5° related to (110) and (1-10) of cellulose-Iβ (ICDD: 00-060-1502) [61], confirming the native cellulose structure in the fresh material. The intensity of the cellulose signal differs between different parts of the plant. However, based on the similar ratio between the intensity of the peak at 22.2° and the intensity of the background signal, we can see that the cellulose content is similar in the stems, leaves and roots, with the packing density being the most important factor influencing the overall intensity. In addition, we observe a peak at 26.5°, which was assigned to the background signal (graphite phase), as it was not observed when analyzing a larger amount of the sample (Appendix A, Fig. A.3). Pyrolysis at 700°C completely changes the structure, lacking the crystalline narrow peaks typical of biochar samples treated at low temperature (< 2000°C). At higher temperatures, a graphite structure with (main) (002) reflection at 26.5° is formed [62], although the temperature of graphitization could be lowered to 1200°C with an inexpensive iron- or magnesium-based catalyst [63]. However, we can observe a consistent shift to higher 2θ (23°-25°) related to turbostratic carbon, which consists of aromatic compounds [64] and is the result of high temperature treatment [65]. Here we show the overlay diffractograms, while the separated spectra can be found in the supporting information (Fig. A.4-5).

Fig. 5 (b) shows the influence of the heating rate on the structure of the pyrolyzed hemp stems. A detailed comparison (Appendix A, Fig. A.2) of the ratios at the average intensity between 20 and 27° (representing

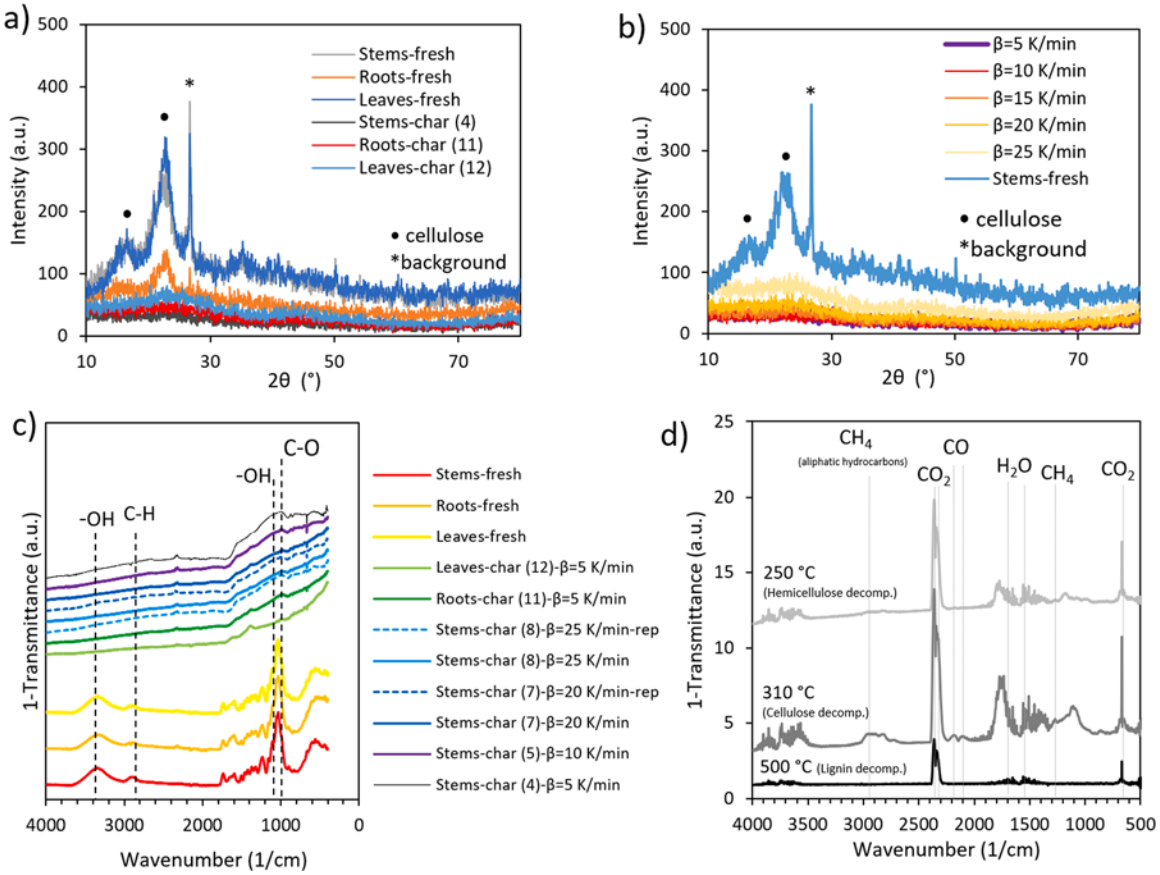

Fig. 5. Comparison of X-ray powder diffractograms of fresh and pyrolyzed samples of stems, roots and leaves prepared at a heating rate of 5 K/min (a), X-ray powder diffractograms of fresh and pyrolyzed hemp stems (samples 4-8) pyrolyzed at 5 K/min (b), ATR-FTIR of fresh and pyrolyzed hemp samples (c; The spectra are evenly distributed along the Y-axis for easier comparison.), FTIR of gas compounds during pyrolysis of hemp stems at 5 K/min at three different temperatures related to the degradation of hemicellulose, cellulose and lignin (d; The spectra are evenly distributed along the Y-axis for easier comparison.).

the turbostratic carbon) and the background signal (average between 60°-70°) shows a decreasing trend in the signal intensity of the partially ordered carbon at lower heating rates. In other words, this suggests that prolonged exposure to higher temperatures damages the turbostratic structure, which is unlikely [64]. Another possibility is that increasing the heating rate promotes the formation of this structure. This could be the result of different kinetics of the polymerization reactions, where aromatic layers are formed, compared to the kinetics of the decomposition reactions, where gaseous products are observed. We can also see this from the fact that the final char yield after pyrolysis at 5 K/min is lower than at higher heating rates. Further tests would need to be performed to test other possible hypotheses (altered interaction of gaseous products with solids, etc.)

3.6.4. ATR-FTIR of solid samples

The functional groups were compared by ATR-FTIR (Fig. 5 c). Although different O/C ratios of the different hemp parts were detected by SEM-EDS, the FTIR spectrum is similar. The FTIR spectra of the resulting biochar are also similar between the different plant parts. When comparing the FTIR spectra of fresh and pyrolyzed hemp, a strong decrease in the peaks at 3370 cm^{-1} and 1050 cm^{-1} (related to -OH) and 980 cm^{-1} (related to C-O) and 2900 cm^{-1} (related to C-H) was observed, which is to be expected in the formation of biochar [64].

3.6.5. FTIR of the gaseous products

The gaseous pyrolysis products were also determined *in situ* by FTIR by heating the stems sample in the flow of N_2 at a rate of 5 K/min. It can be seen that at 250°C CO_2 and H_2O are formed with minor presence of CO and CH_4. When the temperature is increased, the cellulose is broken down at around 310°C, producing larger amounts of methane and carbon monoxide. With a further increase in temperature to 500°C, lignin decomposition becomes the predominant cause of the change in solid mass, leading to the formation of CO_2 and H_2O, while other gasses cannot be detected, mainly due to the low intensity and lower mass change, as can be observed in Fig. 5 (d).

4. Conclusions

Kinetic modeling of pyrolysis of industrial hemp biomass considering internal heat transfer and chemical kinetics of four pseudo-components with 1st reaction order was able to accurately (coefficient of determination $\geq$ 0.9968) describe the experimental data from thermogravimetric (TG) measurements in nitrogen atmosphere. The integrated kinetics-transport pyrolysis modelling in our study was based on the actual physics and chemistry during the process, which was not the case in some other literature studies where different kinetic parameters are associated with the change in heating rate or conversion level of the material. This robust modelling approach for pyrolysis could prove useful in the pyrolysis of similar biomass residues as it can be applied to different process conditions, for example: gas flow rate, heating rate and particle size.

The characterizations of industrial hemp biomass and biochar revealed the typical differences in O/C ratio (SEM-EDS), functional groups present (ATR-FTIR) and nanoscale structure (XRD). Elemental analysis showed that Cd, Pb and Zn were present in the roots in lower amounts than in the soil, while the leaves and stems contained no measurable amounts of these elements. Contrary to expectations, the concentration of pollutants in the solid fraction after pyrolysis decreased compared to the predicted value, which was rationalized by the reduction of metal oxides (or salts) to elemental form and evaporation. This type of pyrolysis could be used to treat biomass with high heavy metal content with cleaning of the gas phase by condensation and producing agricultural-grade biochar, CO-rich gas and a highly concentrated heavy metal stream (e.g. in an absorbent). This can be applied to the pyrolysis of other hyper-(heavy metal)-accumulating plants, while stems and leaves of industrial hemp can be used directly (e.g. in textiles) for further processing as they do not contain significant amounts of pollutants, even if the plant was grown on contaminated soil.

Author statement

We declare that this manuscript is original, has not been published before and is not currently being considered for publication elsewhere.

We confirm that the manuscript has been read and approved by all named authors and that there are no other persons who satisfied the criteria for authorship but are not listed. We further confirm that the order of authors listed in the manuscript has been approved by all of us.

We understand that the Corresponding Author is the sole contact for the Editorial process. He is responsible for communicating with the other authors about progress, submissions of revisions and final approval of proofs.

CRediT authorship contribution statement

Jure Voglar: Writing – review & editing, Writing – original draft, Visualization, Software, Methodology, Investigation, Formal analysis, Data curation, Conceptualization. **Anže Prašnikar:** Writing – review & editing, Writing – original draft, Visualization, Methodology, Investigation, Formal analysis, Data curation. **Konstantin Moser:** Writing – review & editing, Investigation, Formal analysis. **Elisa Carlon:** Writing – review & editing, Supervision, Methodology, Investigation. **Manuel Schwabl:** Writing – review & editing, Supervision, Formal analysis. **Blaž Likozar:** Writing – review & editing, Writing – original draft, Supervision, Methodology, Investigation, Funding acquisition, Conceptualization.

Declaration of competing interest

The authors declare that they have no known competing financial interests or personal relationships that could have appeared to influence the work reported in this paper.

Acknowledgements

J.V. thanks Mr. David Geršak from the Konopko Cooperative - Slovenian Hemp Cooperative for providing the biomass samples and the data associated with its cultivation and processing.

B.L. thanks the support from the Slovenian Research and Innovation Agency through core funding P2-0152 and project funding J7-4638.

This research received funding within the BioTrainValue project. BioTrainValue (BIOmass Valorisation via Superheated Steam Torrefaction, Pyrolysis, Gasification Amplified by Multidisciplinary Researchers TRAINing for Multiple Energy and Products' Added VALUEs), with the project number: 101086411, funded by the Horizon Europe's Maria Skłodowska-Curie Staff Exchange program.

Supplementary materials

Supplementary material associated with this article can be found, in the online version, at doi:10.1016/j.tca.2024.179899.

Data availability

Data will be made available on request.

References

[1] A.C. Dietz, J.L. Schnoor, Advances in phytoremediation, Environ. Health Perspect. 109 (2001) 163–168.

[2] E.L. Arthur, P.J. Rice, P.J. Rice, T.A. Anderson, S.M. Baladi, K.L.D. Henderson, J. R. Coats, Phytoremediation—an overview, CRC. Crit. Rev. Plant Sci. 24 (2005) 109–122.

[3] P.K. Padmavathiamma, L.Y. Li, Phytoremediation technology: hyper-accumulation metals in plants, Water. Air. Soil. Pollut. 184 (2007) 105–126.
[4] H. Sarma, Metal hyperaccumulation in plants: a review focusing on phytoremediation technology, Journal of Environmental Science and Technology 4 (2011) 118–138.
[5] K. Prabakaran, J. Li, A. Anandkumar, Z. Leng, C.B. Zou, D. Du, Managing environmental contamination through phytoremediation by invasive plants: A review, Ecol Eng 138 (2019) 28–37, https://doi.org/10.1016/j.ecoleng.2019.07.002.
[6] E. Pilon-Smits, M. Pilon, Phytoremediation of metals using transgenic plants, CRC. Crit. Rev. Plant Sci. 21 (2002) 439–456.
[7] H.T. Rheay, E.C. Omondi, C.E. Brewer, Potential of hemp (Cannabis sativa L.) for paired phytoremediation and bioenergy production, GCB Bioenergy 13 (2021) 525–536.
[8] R. Ahmad, Z. Tehsin, S.T. Malik, S.A. Asad, M. Shahzad, M. Bilal, M.M. Shah, S. A. Khan, Phytoremediation potential of hemp (Cannabis sativa L.): identification and characterization of heavy metals responsive genes, CLEAN–Soil, Air, Water 44 (2016) 195–201.
[9] E.E. Golia, J. Bethanis, N. Ntinopoulos, G.-G. Kaffe, A.A. Komnou, C. Vasilou, Investigating the potential of heavy metal accumulation from hemp. The use of industrial hemp (Cannabis Sativa L.) for phytoremediation of heavily and moderated polluted soils, Sustain. Chem. Pharm. 31 (2023) 100961, https://doi.org/10.1016/j.scp.2022.100961.
[10] H.T. Rheay, E.C. Omondi, C.E. Brewer, Potential of hemp (Cannabis sativa L.) for paired phytoremediation and bioenergy production, GCB Bioenergy 13 (2021) 525–536.
[11] G. Todde, G. Carboni, S. Marras, M. Caria, C. Sirca, Industrial hemp (Cannabis sativa L.) for phytoremediation: Energy and environmental life cycle assessment of using contaminated biomass as an energy resource, Sustainable Energy Technologies and Assessments 52 (2022) 102081, https://doi.org/10.1016/j.seta.2022.102081.
[12] J. Liu, X. Chen, W. Chen, M. Xia, Y. Chen, H. Chen, K. Zeng, H. Yang, Biomass pyrolysis mechanism for carbon-based high-value products, Proceedings of the Combustion Institute 39 (2023) 3157–3181, https://doi.org/10.1016/j.proci.2022.09.063.
[13] V.-N. Edgar, F.-L. Fabián, P.-C.J. Mario, V.-R. Ileana, Coupling plant biomass derived from phytoremediation of potential toxic-metal-polluted soils to bioenergy production and high-value by-products—A review, Applied Sciences 11 (2021) 2982.
[14] A.K. Vuppaladadiyam, S.S.V. Vuppaladadiyam, A. Awasthi, A. Sahoo, S. Rehman, K.K. Pant, S. Murugavelh, Q. Huang, E. Anthony, P. Fennel, S. Bhattacharya, S.-Y. Leu, Biomass pyrolysis: A review on recent advancements and green hydrogen production, Bioresour. Technol. 364 (2022) 128087, https://doi.org/10.1016/j.biortech.2022.128087.
[15] J. Zhou, L.H. Chen, L. Peng, S. Luo, Q.R. Zeng, Phytoremediation of heavy metals under an oil crop rotation and treatment of biochar from contaminated biomass for safe use, Chemosphere 247 (2020) 125856.
[16] S. Huang, J. Liu, S. Chen, J. Wang, Z. Chen, F. Evrendilek, T. Chen, W. Huang, W. Xie, S. Sun, Converting and valorizing heavy metal-laden post-harvest hyperaccumulator (Pteris vittate L.) into biofuel via acid-pretreated pyrolysis and gasification, Chemical Engineering Journal 468 (2023) 143490.
[17] S. Huang, Z. Huang, Z. Chen, J. Wang, F. Evrendilek, J. Liu, Y. He, Y. Ninomiya, W. Xie, G. Zhuang, Simultaneous optimizations of heavy metal immobilizations, products, temperature, and atmosphere dependency by acid pretreatment-assisted pyrolysis and gasification of hyperaccumulator (Pteris vittate L.) biomass, J. Clean. Prod. 450 (2024) 142004.
[18] J. Du, L. Zhang, S. Song, R. Li, R. Xiao, D. Guo, A. Ali, X. Liu, W. Guan, Z. Zhang, Effect of potentially toxic metals (PTMs) on the thermal decomposition of phytoremediation plant wastes: Thermokinetic and gas evolution analysis by TG-DTG-MS, Bioresour. Technol. 293 (2019) 122027, https://doi.org/10.1016/j.biortech.2019.122027.
[19] A. Asghar, R. Haider, C.-G. Liu, M. Afzal, M.A. Mehmood, Evaluating bioenergy potential of the Para grass (Brachiaria mutica) biomass produced on a land-free cultivation system while keeping the water-energy-environment nexus sustainable, Energy Convers. Manage 245 (2021) 114590, https://doi.org/10.1016/j.enconman.2021.114590.
[20] H.P. Nath, B.K. Dutta, N. Bhuyan, B.K. Saikia, N. Saikia, A comprehensive study on the transition metal–catalysed pyrolysis kinetics, thermodynamics and mechanisms of bamboo powder, BioMass Convers. Biorefin. 13 (2023) 5043–5057, https://doi.org/10.1007/s13399-021-01528-4.
[21] J. Du, L. Zhang, T. Liu, R. Xiao, R. Li, D. Guo, L. Qiu, X. Yang, Z. Zhang, Thermal conversion of a promising phytoremediation plant (Symphytum officinale L.) into biochar: Dynamic of potentially toxic elements and environmental acceptability assessment of the biochar, Bioresour. Technol. 274 (2019) 73–82, https://doi.org/10.1016/j.biortech.2018.11.077.
[22] P. Giudicianni, S. Pindozzi, C.M. Grottola, F. Stanzione, S. Faugno, M. Fagnano, N. Fiorentino, R. Ragucci, Pyrolysis for exploitation of biomasses selected for soil phytoremediation: Characterization of gaseous and solid products, Waste Management 61 (2017) 288–299, https://doi.org/10.1016/j.wasman.2017.01.031.
[23] J. He, V. Strezov, R. Kumar, H. Weldekidan, S. Jahan, B.H. Dastjerdi, X. Zhou, T. Kan, Pyrolysis of heavy metal contaminated Avicennia marina biomass from phytoremediation: Characterisation of biomass and pyrolysis products, J. Clean. Prod. 234 (2019) 1235–1245, https://doi.org/10.1016/j.jclepro.2019.06.285.
[24] Z. Al Chami, N. Amer, K. Smets, J. Yperman, R. Carleer, S. Dumontet, J. Vangronsveld, Evaluation of flash and slow pyrolysis applied on heavy metal contaminated Sorghum bicolor shoots resulting from phytoremediation, BioMass BioEnergy 63 (2014) 268–279, https://doi.org/10.1016/j.biombioe.2014.02.027.
[25] Z. Han, Z. Guo, Y. Zhang, X. Xiao, Z. Xu, Y. Sun, Adsorption-pyrolysis technology for recovering heavy metals in solution using contaminated biomass phytoremediation, Resour. Conserv. Recycl. 129 (2018) 20–26, https://doi.org/10.1016/j.resconrec.2017.10.003.
[26] Y. Huang, D.T. Sekyere, J. Zhang, Y. Tian, Fast pyrolysis behaviors of biomass with high contents of ash and nitrogen using TG-FTIR and Py-GC/MS, J. Anal. Appl. Pyrolysis. 170 (2023) 105922, https://doi.org/10.1016/j.jaap.2023.105922.
[27] J.C. Ang, J.Y. Tang, B.Y.H. Chung, J.W. Chong, R.R. Tan, K.B. Aviso, N. G. Chemmangattuvalappil, S. Thangalazhy-Gopakumar, Development of predictive model for biochar surface properties based on biomass attributes and pyrolysis conditions using rough set machine learning, BioMass BioEnergy 174 (2023) 106820, https://doi.org/10.1016/j.biombioe.2023.106820.
[28] Y. Wang, B. Li, A. Gao, K. Ding, X. Xing, J. Wei, Y. Huang, J. Chun-Ho Lam, K. A. Subramanian, S. Zhang, Volatile-char interactions during biomass pyrolysis: Effect of biomass acid-washing pretreatment, Fuel 340 (2023) 127496, https://doi.org/10.1016/j.fuel.2023.127496.
[29] H. Zhang, M. Liu, Y. Yang, W. Chen, J. Zhu, S. Zhang, H. Yang, H. Chen, Y. Chen, Mechanism study on the interaction between holocellulose and lignin during secondary pyrolysis of biomass: In terms of molecular model compounds, Fuel Processing Technology 244 (2023) 107701, https://doi.org/10.1016/j.fuproc.2023.107701.
[30] S. Zhang, Y. Dong, G. Qi, TG-GC-MS study of pyrolysis characteristics and kinetic analysis during different kinds of biomass, Int. J. Hydrogen. Energy 48 (2023) 11171–11179, https://doi.org/10.1016/j.ijhydene.2022.11.333.
[31] D. Han, X. Yang, R. Li, Y. Wu, Environmental impact comparison of typical and resource-efficient biomass fast pyrolysis systems based on LCA and Aspen Plus simulation, J. Clean. Prod. 231 (2019) 254–267, https://doi.org/10.1016/j.jclepro.2019.05.094.
[32] A. Anca-Couce, A. Berger, N. Zobel, How to determine consistent biomass pyrolysis kinetics in a parallel reaction scheme, Fuel 123 (2014) 230–240, https://doi.org/10.1016/j.fuel.2014.01.014.
[33] H. Egnér, H. Riehm, W.R. Domingo, Untersuchungen über die chemische Bodenanalyse als Grundlage für die Beurteilung des Nährstoffzustandes der Böden. II, Chemische Extraktionsmethoden Zur Phosphor-Und Kaliumbestimmung, Kungliga Lantbrukshögskolans Annaler 26 (1960) 199–215.
[34] HEMP IT - FÉDORA 17, (n.d.). https://www.hemp-it.coop/en/produit/hemp-fedora-17/ (accessed December 21, 2023).
[35] NORTHEAST HERITAGE - Fedora 17, (n.d.). https://northeastheritage.com/product/fedora-17/ (accessed December 21, 2023).
[36] N. Stevulova, J. Cigasova, A. Estokova, E. Terpakova, A. Geffert, F. Kacik, E. Singovszka, M. Holub, Properties characterization of chemically modified hemp hurds, Materials 7 (2014) 8131–8150.
[37] S.M.Q. Bokhari, K. Chi, J.M. Catchmark, Structural and physico-chemical characterization of industrial hemp hurd: Impacts of chemical pretreatments and mechanical refining, Ind. Crops. Prod. 171 (2021) 113818.
[38] L.P. Fennell, D. Boldor, Dielectric and thermal properties of sweet sorghum biomass, Journal of Microwave Power and Electromagnetic Energy 48 (2014) 244–260.
[39] B.V Babu, A.S. Chaurasia, Pyrolysis of biomass: improved models for simultaneous kinetics and transport of heat, mass and momentum, Energy Convers. Manage 45 (2004) 1297–1327.
[40] M. Cardona, D.C. Boffito, G.S. Patience, Thermogravimetric heat and mass transfer: Modeling of bitumen pyrolysis, Fuel 143 (2015) 253–261.
[41] J.E. White, W.J. Catallo, B.L. Legendre, Biomass pyrolysis kinetics: a comparative critical review with relevant agricultural residue case studies, J. Anal. Appl. Pyrolysis. 91 (2011) 1–33.
[42] A. Dufour, B. Ouartassi, R. Bounaceur, A. Zoulalian, Modelling intra-particle phenomena of biomass pyrolysis, Chemical Engineering Research and Design 89 (2011) 2136–2146.
[43] L. Gašparovič, J. Labovský, J. Markoš, L. Jelemenský, Calculation of kinetic parameters of the thermal decomposition of wood by distributed activation energy model (DAEM), Chem. Biochem. Eng. Q. 26 (2012) 45–53.
[44] H.S. Barud, C.A. Ribeiro, J.M.V Capela, M.S. Crespi, S.J.L. Ribeiro, Y. Messadeq, Kinetic parameters for thermal decomposition of microcrystalline, vegetal, and bacterial cellulose, J. Therm. Anal. Calorim. 105 (2011) 421–426.
[45] J. Kristanto, M.M. Azis, S. Purwono, Multi-distribution activation energy model on slow pyrolysis of cellulose and lignin in TGA/DSC, Heliyon. 7 (2021).
[46] A.I. Osman, T.J. Young, C. Farrell, J. Harrison, A.H. Al-Muhtaseb, D.W. Rooney, Physicochemical characterization and kinetic modeling concerning combustion of waste berry pomace, ACS. Sustain. Chem. Eng. 8 (2020) 17573–17586.
[47] A.I. Osman, S. Fawzy, C. Farrell, H. Ala'a, J. Harrison, S. Al-Mawali, D.W. Rooney, Comprehensive thermokinetic modelling and predictions of cellulose decomposition in isothermal, non-isothermal, and stepwise heating modes, J. Anal. Appl. Pyrolysis. 161 (2022) 105427.
[48] S. Fawzy, A.I. Osman, C. Farrell, A.H. Al-Muhtaseb, J. Harrison, A.S. Al-Fatesh, A. H. Fakeeha, J. Doran, H. Yang, D.W. Rooney, Characterization and kinetic modeling for pyrolytic conversion of cotton stalks, Energy Sci. Eng. 9 (2021) 1908–1918.
[49] J.A. Ippolito, L. Cui, C. Kammann, N. Wrage-Mönnig, J.M. Estavillo, T. Fuertes-Mendizabal, M.L. Cayuela, G. Sigua, J. Novak, K. Spokas, Feedstock choice, pyrolysis temperature and type influence biochar characteristics: a comprehensive meta-data analysis review, Biochar. 2 (2020) 421–438.
[50] P. Chaowana, W. Hnoocham, S. Chaiprapat, P. Yimlamai, K. Chitbanyong, K. Wanitpinyo, T. Chaisan, Y. Paopun, S. Pisutpiched, S. Khantayanuwong,

Utilization of hemp stalk as a potential resource for bioenergy, Mater. Sci. Energy Technol. 7 (2024) 19–28.
[51] A. Prašnikar, B. Likozar, Sulphur poisoning, water vapour and nitrogen dilution effects on copper-based catalyst dynamics, stability and deactivation during CO 2 reduction reactions to methanol, React. Chem. Eng. 7 (2022) 1073–1082.
[52] X. Shen, M. Dai, J. Yang, L. Sun, X. Tan, C. Peng, I. Ali, I. Naz, A critical review on the phytoremediation of heavy metals from environment: Performance and challenges, Chemosphere 291 (2022) 132979.
[53] Y. Sun, D. Zhang, F. Li, H. Tao, M. Li, L. Mao, Z. Gu, Z. Ling, H. Shi, The rainfall effect onto solidification and stabilization of heavy metal-polluted sediments, R. Soc. Open. Sci. 7 (2020) 192234.
[54] N. Teutsch, Y. Erel, L. Halicz, O.A. Chadwick, The influence of rainfall on metal concentration and behavior in the soil, Geochim. Cosmochim. Acta 63 (1999) 3499–3511.
[55] J. Zhou, L.H. Chen, L. Peng, S. Luo, Q.R. Zeng, Phytoremediation of heavy metals under an oil crop rotation and treatment of biochar from contaminated biomass for safe use, Chemosphere 247 (2020) 125856.
[56] L. Zhang, X. Zhang, K. Qian, Z. Li, Y. Cheng, L.L. Daemen, Z. Wu, W. Huang, Activation and surface reactions of CO and H2 on ZnO powders and nanoplates under CO hydrogenation reaction conditions, J. Energy Chem. 50 (2020) 351–357.
[57] A. Rukini, M.A. Rhamdhani, G.A. Brooks, A. Van den Bulck, Lead Recovery From PbO Using Hydrogen as a Reducing Agent, Metallurgical and Materials Transactions B 54 (2023) 996–1016.
[58] T. Huang, Y. Tang, S. Wang, C. Zhang, X. Ma, Volatilization characteristics and risk evaluation of heavy metals during the pyrolysis and combustion of rubber waste without or with molecular sieves, Ecotoxicol. Environ. Saf. 198 (2020) 110677.
[59] A.I. Osman, S. Fawzy, M. Farghali, M. El-Azazy, A.M. Elgarahy, R.A. Fahim, M.I.A. A. Maksoud, A.A. Ajlan, M. Yousry, Y. Saleem, Biochar for agronomy, animal farming, anaerobic digestion, composting, water treatment, soil remediation, construction, energy storage, and carbon sequestration: a review, Environ. Chem. Lett. 20 (2022) 2385–2485.
[60] Carbon Standards International (CSI), European Biochar Certificate - Guidelines for a Sustainable Production of Biochar, (n.d.). https://www.european-biochar.org/media/doc/2/version_en_10_3.pdf (accessed October 2, 2024).
[61] Y. Nishiyama, P. Langan, H. Chanzy, Crystal structure and hydrogen-bonding system in cellulose Iβ from synchrotron X-ray and neutron fiber diffraction, J. Am. Chem. Soc. 124 (2002) 9074–9082.
[62] S. Mahmood, Z. Ahmad, T. Mahmood, Z.A. Nizami, Graphene oxide synthesis by facile method and its characterization, Open Journal of Chemistry 2 (2019) 11–15.
[63] L. Lower, S.C. Dey, T. Vook, M. Nimlos, S. Park, W.J. Sagues, Catalytic Graphitization of Biocarbon for Lithium-Ion Anodes: A Minireview, ChemSusChem. 16 (2023) e202300729.
[64] C. Zhang, L. Chao, Z. Zhang, L. Zhang, Q. Li, H. Fan, S. Zhang, Q. Liu, Y. Qiao, Y. Tian, Pyrolysis of cellulose: Evolution of functionalities and structure of bio-char versus temperature, Renewable and Sustainable Energy Reviews 135 (2021) 110416.
[65] E. Pusceddu, Comparison between ancient and fresh biochar samples, a study on the recalcitrance of carbonaceous structures during soil incubation, International Journal of New Technology and Research 3 (2017) 39–46.